Structural changes of pulled vesicles: A Brownian dynamics simulation

Hiroshi Noguchi* and Masako Takasu†

Department of Applied Molecular Science, Institute for Molecular Science, Okazaki 444-8585, Japan
(Received 27 November 2001; published 8 May 2002)

We studied the structural changes of bilayer vesicles induced by mechanical forces using a Brownian dynamics simulation. Two nanoparticles, which interact repulsively with amphiphilic molecules, are put inside a vesicle. The position of one nanoparticle is fixed, and the other is moved by a constant force as in optical-trapping experiments. First, the pulled vesicle stretches into a pear or tube shape. Then the inner monolayer in the tube-shaped region is deformed, and a cylindrical structure is formed between two vesicles. After stretching the cylindrical region, fission occurs near the moved vesicle. Soon after this the cylindrical region shrinks. The trapping force ~ 100 pN is needed to induce the formation of the cylindrical structure and fission.

I. INTRODUCTION

Amphiphilic molecules such as lipids and detergents form various structures such as micelles, cylindrical structures, and bilayer membranes in aqueous solution [1]. In particular, closed bilayer membranes, vesicles, are important biologically as model systems for the plasma membrane and intracellular compartments in living cells. The fusion and fission of membranes are essential events in various biological processes [1–5]. In an endocytosis pathway, small vesicles pinch off from the plasma membrane and fuse with lysosomes. Between the plasma membrane and Golgi apparatus, proteins and lipids are carried by vesicles.

Various morphological changes of vesicles are understood via coarse-grained surface models where the bilayer membrane is treated as a smooth continuous surface [1,6–10]. However, in these models, artificial recombination of surfaces is needed to investigate the phenomena accompanying topological change such as fission [9]. These methods provide no information on structural change with molecular resolution. On the other hand, molecular dynamics simulations with atomic resolution have been applied only for ~ 10 ns dynamics of 1000 lipid molecules due to the restrictions of computational time [11–13]. Thus, some authors [14–16] have studied the statics and dynamics of amphiphiles using coarse-grained molecular models. In Ref. [16], the modes of bending undulations and protrusions of amphiphilic molecules in bilayer membranes are distinguished, and the bending rigidity is calculated from the undulations. However, the dynamics of molecular structures under topological changes of vesicles remains unclear.

Recently, we proposed a simple model of amphiphilic molecules to investigate the structural change with molecular resolution [17–19]. We used three-dimensional Brownian dynamics. An amphiphilic molecule is modeled as a rigid rod. Solvent molecules are not taken into account explicitly, and ''hydrophobic'' interaction is mimicked by the local density potential of the hydrophobic segments. The amphiphilic

molecules form a bilayer vesicle in a fluid phase [17].

We clarified spontaneous fusion pathways of two vesicles at two different temperatures [18]. At the high temperature, amphiphilic molecules frequently protrude, and the vesicles contacted form a stalk intermediate, a necklike structure which only connects outer monolayers, as proposed in the stalk models [20–22]. Then a fusion pore opens through a stalk-bending process: a small pore on a vesicle opens next to the elliptic stalk, and the stalk bends around the pore. Then a fusion pore connecting the insides of the vesicles opens. At the lower temperature, the vesicles are stable, and the vesicles contacted do not form the stalk intermediate. We simulated the pore-opening process starting with the stalk intermediates. Some vesicles fuse through the pathway predicted by the modified stalk model [21]: the inner monolayers contact inside the radially expanded stalk, and a fusion pore opens. However, the other vesicles remain in stalk intermediates for many time steps. In Ref. [19], we show that a nanoparticle that interacts attractively with the hydrophilic segments induces fusion-pore opening through a stalk-bending process at these stabilized stalk intermediates. We also studied the fission process induced by the adhesion of the nanoparticle [19].

In our present paper, we investigate the structural changes of a vesicle pulled by mechanical forces: stalk formation and fission. Recent developments of experimental techniques such as optical [23–27] and magnetic [28,29] tweezers make it possible to trap, manipulate, and displace biological objects. Some authors [24–26] reported morphological changes of cells pulled using optical tweezers with beads as local handles. Two beads are attached to the cell at opposite ends of a diameter, and one is held in place with one trap, while the other is moved with a second trap to induce tension in the cell [25,26]. We discuss the experimental conditions needed to observe the simulated structural changes.

This paper is organized as follows. In Sec. II, we describe our simulation model and methodology. The results are presented in Sec. III. Discussion and conclusions are given in Sec. IV and Sec. V, respectively.

II. METHOD

An amphiphilic molecule is modeled as one hydrophilic segment ($j=1$) and two hydrophobic segments ($j=2,3$), which are separated by a fixed distance σ and fixed on a line.

---

*Electronic address: noguchi@ims.ac.jp

†Present address: Department of Computational Science, Kanazawa Univrsity, Kakuma Kanazawa 920-1192, Japan.

The particles manipulated by tweezers are modeled as nano-particles with radius r_{np}. One nanoparticle is fixed at the origin (0,0,0). The other nanoparticle is fixed on the x axis: $(X_{mp},0,0)$, and is moved by a constant external force f_{ex}. The motion of the jth segment of the ith molecule and the moved nanoparticle follows the underdamped Langevin equation:

$$m\frac{d^2\mathbf{r}_{i,j}}{dt^2} = -\zeta\frac{d\mathbf{r}_{i,j}}{dt} + \mathbf{g}_{i,j}(t) - \frac{\partial U}{\partial \mathbf{r}_{i,j}}, \qquad (1)$$

$$m_{mp}\frac{d^2 X_{mp}}{dt^2} = -\zeta_{mp}\frac{dX_{mp}}{dt} + g_{mp}(t) - \frac{\partial U}{\partial X_{mp}} + f_{ex}, \qquad (2)$$

where $m(m_{mp})$ and ζ (ζ_{mp}) are the mass and the friction constant of the segments of molecules (the nanoparticle), respectively. $\mathbf{g}_{i,j}(t)$ and $g_{mp}(t)$ are Gaussian white noise and obey the fluctuation-dissipation theorem. The equations for the translational and the rotational motion of molecules are integrated by the leapfrog algorithm with a time step of $\Delta t = 0.01$ [30]. U is the total potential: $U = U_{AM} + U_{NP}$, where U_{AM} is the interaction potential between amphiphilic molecules and U_{NP} is the interaction potential between amphiphilic molecules and nanoparticles.

Amphiphilic molecules ($i = 1, \ldots, N$) interact via a repulsive soft-core potential and an attractive "hydrophobic" potential: $U_{AM} = U_{REP} + U_{HP2} + U_{HP3}$. Both segments have the same soft radius r_{am},

$$U_{REP} = \sum_{i \neq i'} U_{rep}(2r_{am}, |\mathbf{r}_{i,j} - \mathbf{r}_{i',j'}|), \qquad (3)$$

where $U_{rep}(r_0,r)/\varepsilon = \exp\{-20(r-r_0)/\sigma\}$. We cut off $U_{rep}(r_0,r)$ at $r_0 + 0.3\sigma$. U_{HP2} and U_{HP3} are "hydrophobic" potentials of the middle ($j=2$) and end ($j=3$) segments: $U_{HP2} = \Sigma_i U_{hp}(\rho_{i,2})$ and $U_{HP3} = \Sigma_i U_{hp}(\rho_{i,3})$. $\rho_{i,j}$ is the number of hydrophobic segments in the sphere whose radius is approximately 1.9σ:

$$\rho_{i,j} = \sum_{i \neq i', j' = 2,3} h(|\mathbf{r}_{i,j} - \mathbf{r}_{i',j'}|), \qquad (4)$$

where

$$h(r) = \frac{1}{\exp\{20(r/\sigma - 1.9)\} + 1}.$$

The multibody "hydrophobic" interaction is mimicked by the function $U_{hp}(\rho)$ of the local density of hydrophobic segments, since solvent molecules are not taken into account explicitly:

$$U_{hp}(\rho)/\varepsilon = \begin{cases} -0.5\rho & (\rho < \rho^* - 1), \\ 0.25(\rho - \rho^*)^2 - c & (\rho^* - 1 \leq \rho < \rho^*), \\ -c & (\rho^* \leq \rho), \end{cases} \qquad (5)$$
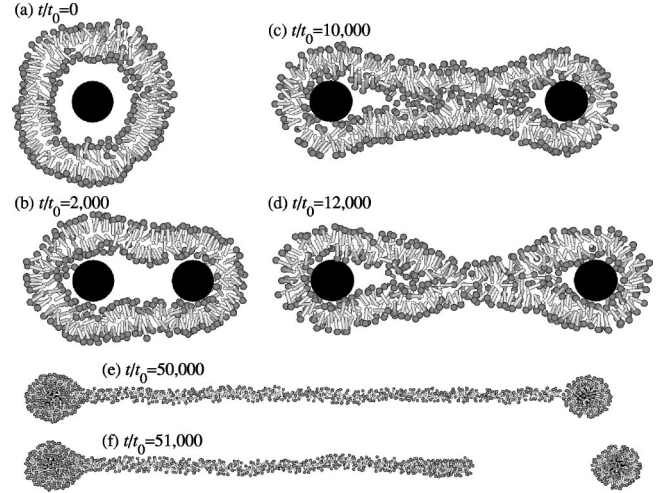

FIG. 1. Snapshots of the vesicle and two nanoparticles at the external force $f_{ex} = 10\varepsilon/\sigma$, $\zeta_{mp}/\zeta = 300$, and $k_B T/\varepsilon = 0.2$. One nanoparticle is fixed at the origin (0,0,0). The other nanoparticle is placed at (0,0,0) at time step $t = 0$, and moves to the right along the x axis. Gray spheres and white cylinders represent hydrophilic and hydrophobic segments of amphiphilic molecules, respectively. Black spheres represent nanoparticles. The snapshots are viewed from the z direction. (a)–(d) Sliced snapshots. Molecules with $-2 \leq z/\sigma < 2$ are shown. (e),(f) All molecules are shown.

where c is given by $c = 0.5\rho^* - 0.25$. We used the values $\rho^* = 10$ and 14 at $j = 2$ and 3, respectively. At low density ($\rho < \rho^* - 1$), $U_{hp}(\rho)$ acts as the pairwise potential $-\varepsilon h(r)$. We assume that the segment is shielded by hydrophobic segments from solvent molecules and hydrophilic segments at ρ^*. Thus, $U_{hp}(\rho)$ is constant at higher density ($\rho \geq \rho^*$). If the pairwise potential $-\varepsilon h(r)$ is used instead of $U_{hp}(\rho)$, the bilayer membrane has no fluid phase and does not form a vesicle spontaneously. We set $h(r) = 1$ for $r < 1.6\sigma$ and $h(r) = 0$ for $r \geq 2.2\sigma$ to save computational time.

Two nanoparticles have a repulsive interaction with amphiphilic molecules. We used the same type of repulsive potential as that between amphiphilic molecules:

$$U_{NP} = \sum_{i,j} U_{rep}(r_{am} + r_{np}, |\mathbf{r}_{i,j} - \mathbf{r}_{np}|). \qquad (6)$$

Nanoparticles do not interact with each other.

At initial states, we set both nanoparticles at the center of mass of a vesicle. We take the standard deviation of three separate runs as an estimate of the calculation error. We present our results with the reduced units $\sigma = 1$, $\varepsilon = 1$, $t_0 = \zeta\sigma^2/\varepsilon = 1$. We fixed the number of molecules $N = 1000$; the radii $r_{am} = 0.5\sigma$ and $r_{mp} = 3\sigma$; the masses $m = m_{mp} = 1$; and the friction constant of segments $\zeta = 1$. We used $\zeta_{mp}/\zeta = 300$ and 1500. When we use $\zeta_{mp}/\zeta = 3$, the moved nanoparticle soon penetrates the membrane of a vesicle. We used $k_B T/\varepsilon = 0.2$ and 0.5, where k_B is the Boltzmann constant and T is the temperature. We mainly describe the results at $k_B T/\varepsilon = 0.2$.

We briefly describe the properties of vesicles at $k_B T/\varepsilon = 0.2$. Amphiphilic molecules spontaneously form vesicles. The vesicle exhibits a clear bilayer structure [see Fig. 1(a)], and is in a fluid phase. Molecules in vesicles diffuse laterally: the lateral diffusion constant is 0.0039 ± 0.0004. Flip-
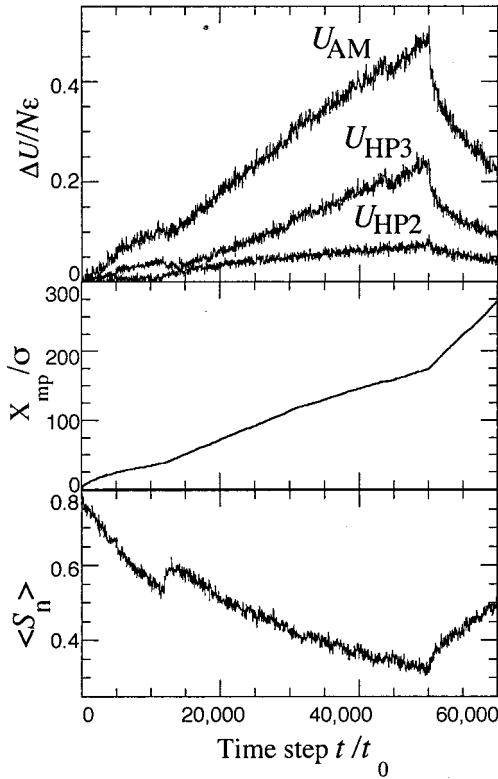
FIG. 2. Time development of the energy, the x coordinate X_{mp} of the moved nanoparticle, and the mean degree of orientation between neighboring molecules $\langle S_n \rangle$ at $f_{ex} = 10\varepsilon/\sigma$ for the data shown in Fig. 1. The energy ΔU equals $U - U^{ini}$, where U^{ini} is the energy without nanoparticles: $U_{AM}^{ini}/N\varepsilon = -11.1999 \pm 0.0006$, $U_{HP2}^{ini}/N\varepsilon = -4.6850 \pm 0.0002$, and $U_{HP3}^{ini}/N\varepsilon = -6.7129 \pm 0.0001$.

flop motion, which is a transverse motion between inner and outer monolayers, is much slower than the lateral diffusion. The half lifetime of flip-flop motion is $\sim 100\,000$ time steps [17]. We estimated the bending rigidity $\kappa/k_B T \simeq 5$ from the fluctuation of quasispherical vesicles and the N dependence of the energy U_{AM} [19]. Under typical experimental conditions, $\kappa/k_B T$ of phospholipid molecules is 5–100 [1]. The simulated vesicles correspond to slightly flexible membranes. The energy needed to form a flat bilayer membrane from isolated amphiphilic molecules $U_{AM}/N/k_B T = -50$ to -60 [19] is on the order of those of typical lipid membranes: $U_{AM}/N/k_B T = -10$ to -30 [31]. Since our model does not explicitly take into account solvent molecules, the volume of vesicles is not fixed. The unit length σ corresponds to ~ 1 nm. The unit time step t_0 corresponds to ~ 1 ns when the lateral diffusion constant is assumed to correspond to that of phospholipids at $30\,^\circ$C, $\sim 10^{-7}$ cm^2/s [32,33]. The unit of external force ε/σ is ~ 20 pN.

III. RESULTS

A pulled vesicle changes its structure. Figure 1 shows sequential snapshots of a vesicle at $f_{ex} = 10\varepsilon/\sigma$, $\zeta_{mp}/\zeta = 300$, and $k_B T/\varepsilon = 0.2$. First, the bilayer vesicle stretches into a pear or tube shape [Figs. 1(b) and 1(c)]. Then the stretched bilayer structure changes to a cylindrical structure
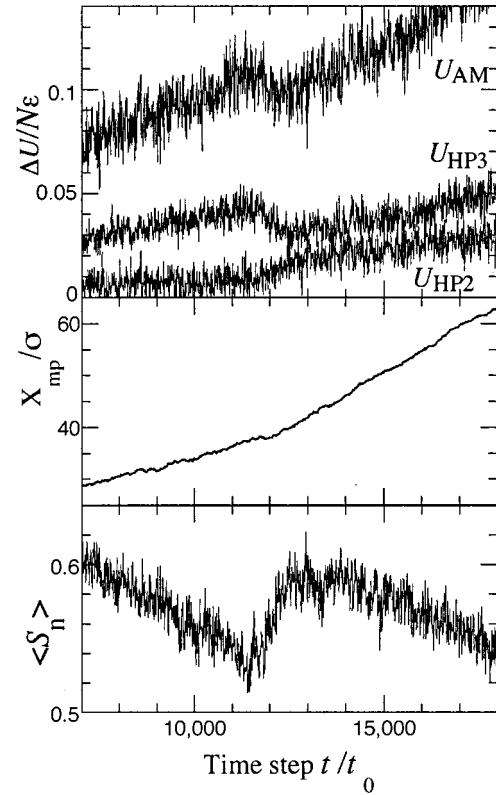

FIG. 3. Enlarged graph of Fig. 2 around stalk formation.

[Fig. 1(d)]. We call this structure a stalk, since it is similar to the stalk intermediates in vesicle fusion [18,20]. The stalk region becomes longer and is broken near the right vesicle [Figs. 1(e) and 1(f)]. Then the stalk region soon shrinks. Figures 2 and 3 show the time development of the energies U_{AM}, U_{HP2}, U_{HP3}, the x coordinate X_{mp} of the moved nanoparticle, and the mean degree of orientation between neighboring molecules $\langle S_n \rangle$. S_n is defined as $S_n = \mathbf{u}_i \mathbf{u}_j$ if $|\mathbf{r}_i - \mathbf{r}_j| < 2$. $\mathbf{r}_i$ and $\mathbf{u}_i$ are the center of mass and the unit orientation vectors of the ith molecule. The average for $\langle S_n \rangle$ is taken over all pairs of neighbors i,j. U_{REP} exhibits similar development to U_{HP3}: a sigmoidal curve appears at $t/t_0 \simeq 12\,000$; $\Delta U_{REP} = 0.042$, 0.083, 0.123, 0.142, and 0.181 at $t/t_0 = 10\,000$, 20\,000, 30\,000, 40\,000, and 50\,000, respectively.

Before stalk formation, the vesicle stretches, and the structures are partially deformed on the membrane pushed by the nanoparticles and on the inner monolayer between nanoparticles. These deformations make those membranes thinner, and the second segments are not exposed. Thus U_{HP2} is almost constant, although U_{HP3} and U_{REP} increase and $\langle S_n \rangle$ decreases. Under pulling tension, the radius of the bilayer tube decreases, and the inner monolayers are in tight contact at $t/t_0 \simeq 8000$ [Fig. 1(c)].

At $t/t_0 \simeq 12\,000$, the inner monolayer in the tube-shaped vesicle is destabilized by pressure from the outer monolayer, and the stalk structure is formed. Figures 4(a)–4(c) show sliced snapshots under stalk formation. The inner monolayer disappears around $x = 20\sigma$, and the amphiphilic molecules move in the $+x$ or $-x$ direction. On the other hand, the
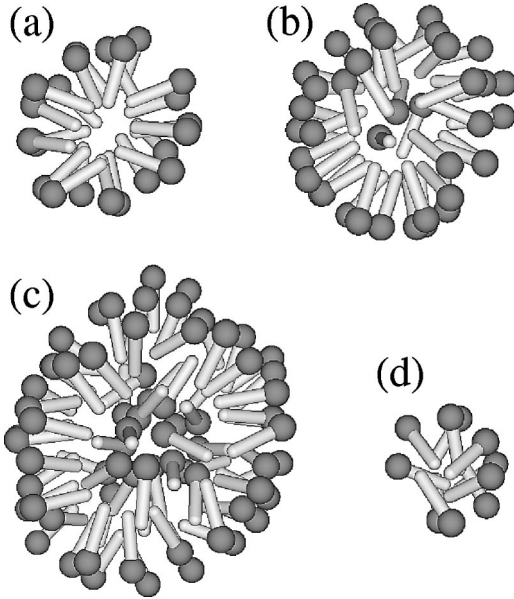
FIG. 4. Sliced snapshots viewed from $-x$ direction at $t/t_0 =$ (a)–(c) 12 000 and (d) 50 000 for the data shown in Fig. 1. Molecules with (a) $20 < x/\sigma \leqslant 24$, (b) $24 < x/\sigma \leqslant 28$, (c) $28 < x/\sigma \leqslant 32$, and (d) $85 < x/\sigma \leqslant 89$ are shown. X_{np}/σ are 37.94 and 173.85 at $t/t_0 = 12\,000$ and 50 000, respectively.

outer monolayer keeps its structure. The inner monolayer divides into two clusters inside the outer monolayer. This pathway is similar to the reverse pathway in the modified stalk model [18,21]. The energies and $\langle S_n \rangle$ exhibit sigmoidal curves as shown in Fig. 3. U_{AM} decreases and the order between neighboring molecules increases under stalk formation. Thus the stalk is formed after obtaining higher energy to overcome the free-energy barrier for formation. We define the time step t_{sta} of stalk formation as the time step when the hydrophilic cluster of the inner monolayer divides into two clusters. The hydrophilic cluster is defined as follows. When a hydrophilic segment is closer than 1.9σ to the hydrophilic segment in a hydrophilic cluster, the segment belongs to the hydrophilic cluster. Although inner and outer monolayers often become one cluster by thermal fluctuation, this effect does not modify t_{sta} much. In this run we obtain $t_{sta}/t_0 = 11\,750$, and the mean time step is $\langle t_{sta} \rangle / t_0 = 10,100 \pm 1400$ for three separate runs. At $f_{ex} = 10\varepsilon/\sigma$, the time step of stalk formation can be decided using another definition such as the peak of U_{AM} or $\langle S_n \rangle$. At higher external force, however, the stalk formation can be detected only using hydrophilic clusters, since their sigmoidal shapes disappear.

After stalk formation, the energies increase, and $\langle S_n \rangle$ decreases with an increase in the stalk region until fission. U_{HP2} also increases since some second segments are exposed in the stalk region. A sliced snapshot of the stalk is shown in Fig. 4(d). Figure 5 shows the density distribution ρ_x along the x axis. The stalk is thinner at larger x, and ρ_x decreases from 3 to 2.5 at $t/t_0 \simeq 47\,500$. Since the nanoparticle moves fast, the stretching stalk does not form a uniform density ρ_x. We distinguish the stalk region, the right moved vesicle, and the left fixed vesicle using ρ_x as follows. We define x_{min} as x with minimum ρ_x in $0 < x < X_{mp}$. Then we define x_{right} (x_{left})
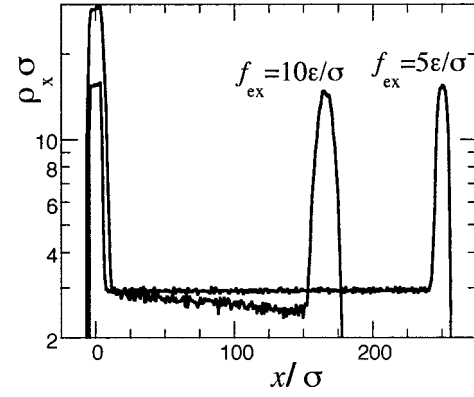

FIG. 5. Density distribution ρ_x along the x axis. The data at $f_{ex} = 5\varepsilon/\sigma$ are averaged for steady stretching vesicles $(t/t_0 = 1\,100\,000 - 1\,300\,000)$ in three runs. The data at $f_{ex} = 10\varepsilon/\sigma$ are averaged for stretching vesicles before fission $(t/t_0 = 45\,000 - 50\,000)$ for the data shown in Fig. 1.

as x where ρ_x first becomes larger than $7/\sigma$ with an increase (decrease) in x from x_{min}. The molecules with $x_i \leqslant x_{left}$, $x_{left} < x_i < x_{right}$, and $x_i \geqslant x_{right}$ belong to the left vesicle, stalk region, and right vesicle, respectively. The numbers of molecules in the left vesicle, stalk region, and right vesicle are N_{left}, N_{sta}, and N_{right}, respectively. The number of molecules in vesicles is $N_{vec} = N_{left} + N_{right}$. We used the molecules in $x_{left} + 5\sigma < x_i < x_{right} - 5\sigma$ to calculate the physical quantities of the stalk, since the region $x_{left} < x_i < x_{right}$ includes the connection points between stalk and vesicles. The number of molecules in this region is N'_{sta}. Figure 6 shows the probability distribution of the orientation degree S_n between neighboring molecules. This distribution exhibits a steep peak at $S_n = 1$ on a vesicle without nanoparticles $(t = 0)$. The amphiphilic molecules are clearly ordered in a bilayer vesicle. As the vesicle stretches, the peak at $S_n = 1$ becomes lower and broader. The small peak at $S_n =$
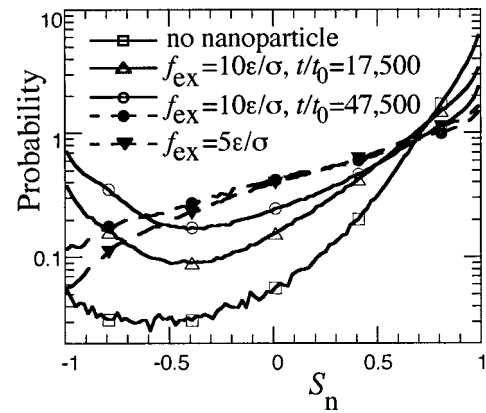

FIG. 6. Probability distribution of the orientation degree between neighboring molecules, S_n. Open symbols with solid lines represent S_n of all molecules. Filled symbols with broken lines represent S_n of molecules in the stalk $(x_{left} + 5\sigma < x_i < x_{right} - 5\sigma)$. The data are averaged for $t/t_0 = 15\,000 - 20\,000$ and $t/t_0 = 45\,000 - 50\,000$ at $f_{ex} = 10\varepsilon/\sigma$; for $t/t_0 = 1\,100\,000 - 1\,300\,000$ at $f_{ex} = 5\varepsilon/\sigma$. The probability is normalized as $\int P(S_n)dS_n = 1$. Symbols are shown for 20 data points.
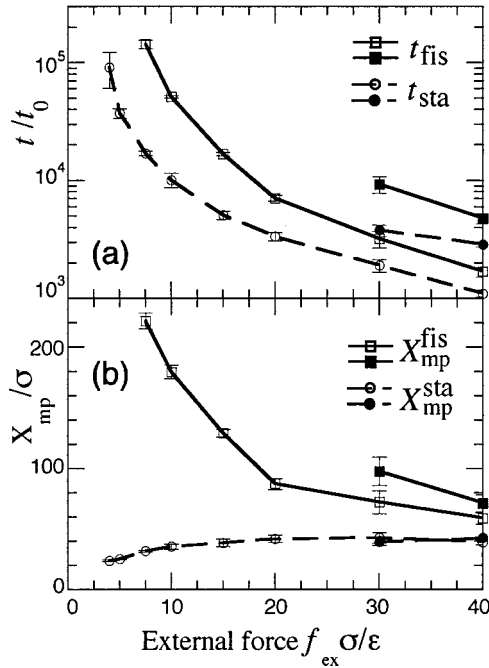
FIG. 7. External force dependence of (a) time steps t and (b) x coordinate X_{mp} of the nanoparticle for fission and stalk formation at $k_B T/\varepsilon = 0.2$. Open and filled symbols represent the results averaged for three runs at $\zeta_{mp}/\zeta = 300$ and 1500, respectively.

FIG. 8. Time development of the energies, the x coordinate X_{mp} of the moved nanoparticle, and the mean density of the stalk ρ_x^{sta} at $f_{ex} = 5\varepsilon/\sigma$, $\zeta_{mp}/\zeta = 300$, and $k_B T/\varepsilon = 0.2$. U_{AM}^{sta} and U_{AM}^{vec} are the mean energies of molecules in the stalk and vesicles, respectively.

-1 represents the existence of an interdigitated structure around nanoparticles, and there is no peak at $S_n = -1$ in the stalk region.

Fission occurs on the stalk with $\rho_x \simeq 2.5$ near the right dragged vesicle. We define the time step t_{fis} of fission as the time step when a hydrophobic cluster divides into two. The hydrophobic cluster is defined as follows [17]. When one of the hydrophobic segments of a molecule is closer than 2σ to at least one of the hydrophobic segments of the molecules in a cluster, the molecule belongs to the cluster. In this run, we obtain $t_{fis}/t_0 = 50\,030$, and the mean time step is $\langle t_{sta} \rangle/t_0 = 52\,000 \pm 2000$ for three separate runs. We call the period between the stalk formation and fission from t_{sta} to t_{fis} the stalk period. After fission, the energies decrease fast under stalk shrinking, and the nanoparticle moves faster since it drags fewer molecules (see Fig. 2).

Figure 7 shows the f_{ex} dependence of (a) t_{sta}, t_{fis}, and (b) X_{mp}. The stalk formation occurs at $f_{ex} \geq 4\varepsilon/\sigma$, and the fission occurs at $f_{ex} \geq 7.5\varepsilon/\sigma$. We observed the same time development in three separate runs except for $f_{ex} = 40\varepsilon/\sigma$ and $\zeta_{mp}/\zeta = 300$. The error bars in Fig. 7, which show the standard deviation of three separate runs, are much less than their f_{ex} dependence. At $f_{ex} = 40\varepsilon/\sigma$ and $\zeta_{mp}/\zeta = 300$, the fission is observed in three runs, and the moved nanoparticle penetrates the membrane before stalk formation in the other three runs. X_{mp}^{sta} is almost independent of f_{ex} and ζ_{mp}. As f_{ex} decreases, a longer stalk becomes more stable, and fission occurs in the longer stalk.

At $f_{ex} = 5\varepsilon/\sigma$, fission does not occur even up to $t/t_0 = 1\,300\,000$ as shown in Fig. 8. After $t/t_0 = 1\,100\,000$, the energies and X_{mp} are almost constant, and the stalk reaches a
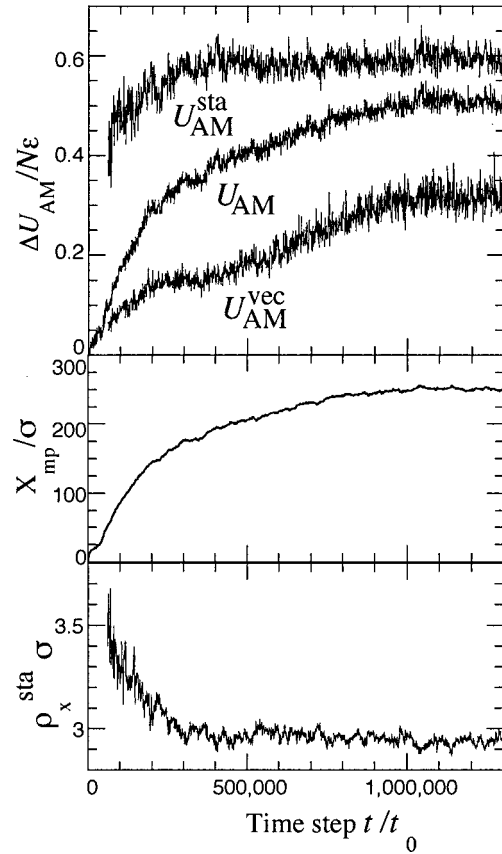
steady state. The amphiphilic molecules are uniformly distributed in the stalk region as shown in Fig. 5, and the mean density of the stalk is $\langle \rho_x^{sta} \rangle \sigma = 2.93 \pm 0.01$. The molecules in the stalk diffuse slowly in the x direction: the diffusion constant is 0.0008 ± 0.0001 in the steady state. This diffusion constant is $1/5$ of that in a bilayer vesicle. The energy U_{AM}^{sta}/N'_{sta} in the stalk region and ρ_x^{sta} reach constant values at $t/t_0 \simeq 400\,000$. The energy U_{AM}^{vec}/N_{vec} in vesicles increases more slowly. When most molecules in the inner monolayer of vesicles are removed, X_{mp} and U_{AM}^{vec}/N_{vec} reach constant values. When f_{ex} is changed from $5\varepsilon/\sigma$ to $7.5\varepsilon/\sigma$ in the steady stalk state, fission occurs in an additional 30 000 time steps.

At $f_{ex} = 3\varepsilon/\sigma$, the stalk is not formed, and vesicles remain pear shaped as shown in Fig. 1(b). Thus the force $f_{ex} > 3\varepsilon/\sigma$ is needed for stalk formation. When the initial state is a stalk state, the stalk with $\langle \rho_x^{sta} \rangle \sigma = 4 \pm 0.5$ remains at $f_{ex} = 3\varepsilon/\sigma$.

Figure 9 shows (a) the mean numbers of molecules in the vesicles and stalk region and (b) the mean velocity V_{sta} of the nanoparticles averaged over the stalk period. V_{sta} is defined as $V_{sta} = (X_{mp}^{fis} - X_{mp}^{sta})/(t_{fis} - t_{sta})$. The mean velocity does not depend on the definition much. We obtained almost the same velocities using a linear least-squares fit. We derive this f_{ex}
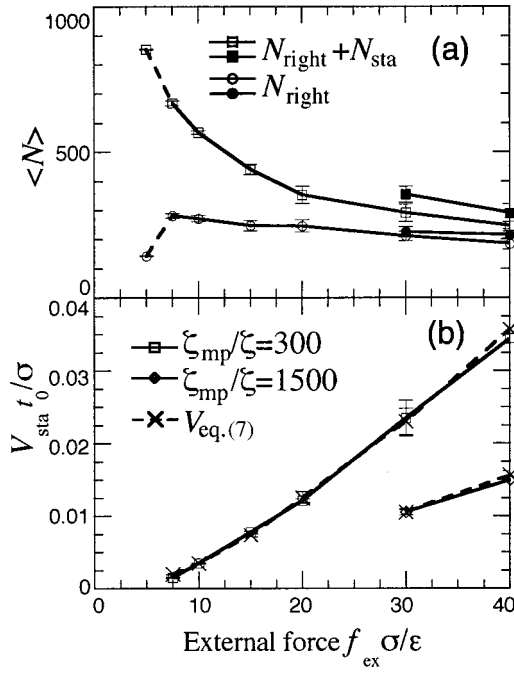
FIG. 9. (a) Mean numbers of molecules in the right dragged vesicle N_{right} and the stalk N_{sta} averaged over the stalk period. The data for $f_{ex}=5\varepsilon/\sigma$ are averaged for steady states ($t/t_0 = 1\,100\,000$–$1\,300\,000$). The number of all molecules is $N=1000$. Open and filled symbols represent the numbers at $\zeta_{mp}/\zeta=300$ and 1500, respectively. (b) Mean velocity V_{sta} of the nanoparticle in the stalk period. $V_{eq.(7)}$ are given by Eq. (7).

dependence of V_{sta} as follows. In steady stretching, the velocity is assumed to be

$$\zeta_{sta}V = f_{ex} - f_{sta}, \qquad (7)$$

where ζ_{sta} and f_{sta} are the mean friction constant and the mean shrinking force in the stalk period, respectively. We estimate $\zeta_{sta}=\zeta_{mp}+(N_{right}+N_{sta})\zeta_{am}$ on the assumption that the nanoparticle drags the molecules in the right vesicle and stalk region. ζ_{am} is the friction constant of the center of the amphiphilic molecules, and $\zeta_{am}=3\zeta$. With an increase in f_{ex}, N_{sta} decreases since fission occurs in the shorter stalk. f_{sta} is derived from differentiation of U_{AM} with respect to X_{mp}. Since we obtained the averaged force $f_{sta}\simeq3\varepsilon/\sigma$ for all f_{ex}, we used $f_{sta}=3\varepsilon/\sigma$ for velocity estimation. The velocities given by Eq. (7) agree well with V_{sta}.

At $k_BT/\varepsilon=0.5$ and $\zeta_{mp}/\zeta=300$, we simulated vesicles pulled by $f_{ex}\sigma/\varepsilon=5$ and 10. The vesicles form a stalk structure through tube-shaped bilayer vesicles. However, they do not divide into two vesicles. A pore opens on the right vesicle and the nanoparticle goes out of the vesicle in all six runs. In three of six runs, the pore opens by the side of a stalk on the right vesicle, and the vesicle opens to a flat membrane, as in opening a hand from a fist. Thus membranes are less stable at $k_BT/\varepsilon=0.5$ than at $k_BT/\varepsilon=0.2$, and the membrane by the side of stalk tends to deform.

IV. DISCUSSION

In our simulation, the forces $f_{ex}\geq4\varepsilon/\sigma$ (~80 pN) and $f_{ex}\geq7.5\varepsilon/\sigma$ (~150 pN) are needed to induce stalk formation and fission, respectively. These forces can be produced experimentally. The maximum forces of optical [23–26] and magnetic [29] tweezers are 100 pN and 10 000 pN, respectively.

Since our model does not explicitly take into account solvent molecules, the volume of the pulled vesicles decreases. In the usual experimental conditions, the volume of a lipid vesicle, a liposome, is fixed osmotically. Hotani *et al.* [6,34–36] reported that a liposome exhibits a ϕ shape, a central ellipsoid and two straight tubes, due to the mechanical force generated by the polymerization of tubulin or actin. This bilayer tube (tether) is also generated in liposomes and cells using optical [24] and magnetic tweezers [28]. Our simulation can be applied to two experimental conditions: water-permeable vesicles and bilayer tubes. In the former case, the stretching dynamics of a vesicle couples with the permeation of water. The stretching rate should strongly depend on the permeation rate. Water can permeate the membranes if there is an osmotic pressure difference between the inside and outside of a vesicle. Liposomes, where aquaporin water channels are reconstructed [37,38], have high permeability for water. The latter is the membrane in the tube region of ϕ-shaped liposomes; we do not incorporate the ellipsoid region explicitly in our model, and its tension is mimicked by the fixed nanoparticle. In this case, forces larger than 100 pN may be needed for stalk formation, to remove water molecules between inner monolayers.

In this paper, we use Brownian dynamics and ignore hydrodynamic interaction. The long-ranged hydrodynamic interactions can accelerate structural changes. Sunil Kumar *et al.* [10] estimated this effect using scaling argument for budding dynamics. This effect should also modify the stretching dynamics of pulled vesicles quantitatively. In particular, this effect is important in stalk formation, since molecules in the inner monolayer flow in the x direction.

Now we discuss the model dependence. In our present model, the stalk structure shows high stability. This stability would depend on the properties of amphiphilic molecules such as tail length and the size of a hydrophilic segment. When a hydrophobic tail consists of three segments, the oriented conformation with larger S_n would be preferred, and the stalk state should become less stable compared to a bilayer membrane. Then fission may occur in shorter stalks. When the radius of a hydrophilic segment is slightly larger than that of hydrophobic segments, the stalks should become more stable. The stability of the stalk structure may be measured by mechanical forces in experimental studies. In some experimental conditions, stretched stalk structures with long lifetime might be obtained.

We used small vesicles and small trapped particles with diameters of 20 and 6 mm, respectively, to save computational time. When larger vesicles and larger particles are used, the simulated structural changes should be slightly modified. The stalk formation and fission will occur at larger

X_{mp}. The particle penetration of the membrane should need larger forces $f_{\mathrm{ex}} > 40\varepsilon/\sigma$.

The stalk is formed by a pulling tension through the reverse pathway in the modified stalk model. On the other hand, the adhesion of a nanoparticle induces structural change from budded states to stalk states through a different pathway [19]: pores open on the membrane in the pinched connection region, and the connection region becomes smaller. The adhering nanoparticle destabilizes both inner and outer monolayers. On the other hand, in the pulled vesicle, the outer monolayer keeps its structure although the inner monolayer is destabilized. Thus the selective destabilization of inner monolayers may be significant to induce structural changes through the pathway of the modified stalk model.

V. CONCLUSION

We have shown the structural changes of a vesicle pulled by mechanical forces. The pulled vesicle stretches, and the inner monolayers contact each other. Then a stalk structure is formed at $f_{\mathrm{ex}} \geq 4\varepsilon/\sigma$ through the reverse pathway of the modified stalk model: the inner monolayer is destabilized, and amphiphilic molecules in the inner monolayer are moved in lateral directions inside the outer monolayer. The stalk region stretches, and fission occurs near the moved vesicle at $f_{\mathrm{ex}} \geq 7.5\varepsilon/\sigma$.

Fusion is also induced by mechanical forces [39]. The nanoparticle is placed inside each vesicle, and is moved by external forces. The membranes are pushed from both sides, and fusion occurs. Our results suggest that these structural changes can be observed in experiments using optical or magnetic tweezers, and the stability of the stalk structure and tube-shaped vesicles may be measured by pulling vesicles.

[1] *Structure and Dynamics of Membranes*, edited by R. Lipowsky and E. Sackmann (Elsevier Science, Amsterdam, 1995).
[2] R. Jahn and T. C. Südhof, Annu. Rev. Biochem. **68**, 863 (1999).
[3] B. B. Allan and W. E. Balch, Science **285**, 63 (1999).
[4] K. Takei and V. Haucke, Trends Cell Biol. **11**, 385 (2001).
[5] B. J. Nichols and J. Lippincott-Schwartz, Trends Cell Biol. **11**, 406 (2001).
[6] H. Hotani, F. Nomura, and Y. Suzuki, Curr. Opin. Colloid Interface Sci. **4**, 358 (1999).
[7] R. Morikawa, Y. Saito, and H. Hyuga, J. Phys. Soc. Jpn. **68**, 1760 (1999).
[8] M. Kraus, W. Wintz, U. Seifert, and R. Lipowsky, Phys. Rev. Lett. **77**, 3685 (1996).
[9] C.-M. Chen, P. G. Higgs, and F. C. MacKintosh, Phys. Rev. Lett. **79**, 1579 (1997).
[10] P. B. Sunil Kumar, G. Gompper, and R. Lipowsky, Phys. Rev. Lett. **86**, 3911 (2001).
[11] L. R. Forrest and M. S. P. Sansom, Curr. Opin. Struct. Biol. **10**, 174 (2000).
[12] S. E. Feller, Curr. Opin. Colloid Interface Sci. **5**, 217 (2000).
[13] S. J. Marrink, E. Lindahl, O. Edholm, and A. E. Mark, J. Am. Chem. Soc. **123**, 8638 (2001).
[14] S. Karaborni *et al.*, Science **266**, 254 (1994).
[15] A. T. Bernardes, J. Phys. II **6**, 169 (1996).
[16] R. Goetz, G. Gompper, and R. Lipowsky, Phys. Rev. Lett. **82**, 221 (1999).
[17] H. Noguchi and M. Takasu, Phys. Rev. E **64**, 041913 (2001).
[18] H. Noguchi and M. Takasu, J. Chem. Phys. **115**, 9547 (2001).
[19] H. Noguchi and M. Takasu, Biophys. J. (to be published).
[20] L. Chernomordik, M. M. Kozlov, and J. Zimmerberg, J. Membr. Biol. **146**, 1 (1995).

[21] D. P. Siegel, Biophys. J. **65**, 2124 (1993).
[22] P. I. Kuzmin, J. Zimmerberg, Yu. A. Chizmadzhev, and F. S. Cohen, Proc. Natl. Acad. Sci. U.S.A. **98**, 7235 (2001).
[23] A. Ashkin, Proc. Natl. Acad. Sci. U.S.A. **94**, 4853 (1997).
[24] J. Dai, M. P. Sheetz, X. Wan, and C. E. Morris, J. Neurosci. **18**, 6681 (1998).
[25] S. Hénon, G. Lenormand, A. Richert, and F. Gallet, Biophys. J. **76**, 1145 (1999).
[26] J. Sleep, D. Wilson, R. Simmons, and W. Gratzer, Biophys. J. **77**, 3085 (1999).
[27] A. Kusumi and Y. Sako, Curr. Opin. Cell Biol. **8**, 566 (1996).
[28] V. Heinrich and R. E. Waugh, Ann. Biomed. Eng. **24**, 595 (1996).
[29] A. R. Bausch, F. Ziemann, A. A. Boulbitch, K. Jacobson, and E. Sackmann, Biophys. J. **75**, 2038 (1998).
[30] M. P. Allen and D. J. Tildesley, *Computer Simulation of Liquids* (Clarendon Press, Oxford, 1987).
[31] C. Tanford, *The Hydrophobic Effect: Formation of Micelles and Biological Membranes*, 2nd ed. (Wiley, New York, 1980).
[32] E.-S. Wu, K. Jacobson, and D. Papahadjopoulos, Biochemistry **16**, 3936 (1977).
[33] W. Pfeiffer, T. Henkel, E. Sackmann, W. Knoll, and D. Richter, Europhys. Lett. **8**, 201 (1989).
[34] H. Hotani and H. Miyamoto, Adv. Biophys. **26**, 135 (1990).
[35] T. Kaneko, T. J. Itoh, and H. Hotani, J. Mol. Biol. **284**, 1671 (1998).
[36] M. Honda, K. Takiguchi, S. Ishikawa, and H. Hotani, J. Mol. Biol. **287**, 293 (1999).
[37] M. L. Zeidel, S. V. Ambudkar, B. L. Smith, and P. Agre, Biochemistry **31**, 7436 (1992).
[38] M. Borgnia, S. Nielsen, A. Engel, and P. Agre, Annu. Rev. Biochem. **68**, 425 (1999).
[39] H. Noguchi (unpublished).